Potential improvements in global carbon flux estimates from a network of laser heterodyne radiometer measurements of column carbon dioxide

Paul I. Palmer,[1,2] Emily L. Wilson,[3] Geronimo L. Villanueva,[3] Giuliano Liuzzi,[3,4] Liang Feng,[1]
Anthony J. DiGregorio,[3,5] Jianping Mao,[3,6] Lesley Ott,[3] Bryan Duncan[3]

[1]National Centre for Earth Observation, University of Edinburgh, Edinburgh, UK
[2]School of Geosciences, University of Edinburgh, Edinburgh, UK
[3]NASA Goddard Space Flight Center, 8800 Greenbelt Road, Greenbelt, MD 20771, USA
[4]Department of Physics, American University, 4400 Massachusetts Avenue NW, Washington, DC 20016, USA
[5]Science Systems and Applications, Inc., Lanham, MD 20706, USA
[6]Earth System Science Interdisciplinary Center, University of Maryland, College Park, MD 20740, USA

Correspondence to: Emily Wilson (Emily.L.Wilson@nasa.gov)

Abstract. We present Observing System Simulation Experiments (OSSEs) to evaluate the impact of a new network of ground-based miniaturized laser heterodyne radiometer (mini-LHR) instruments that measure atmospheric column-averaged carbon dioxide (XCO_2) with high precision (1 ppm). A particular strength of this passive measurement approach is its insensitivity to clouds and aerosols due to its direct sun pointing and narrow field-of-view (0.2 degrees). Developed at NASA Goddard Space Flight Center (GSFC), these portable, low-cost mini-LHR instruments were designed to operate in tandem with the sun photometers used by the AErosol RObotic NETwork (AERONET). This partnership allows us to leverage the existing framework of AERONET's 500+ site global ground network, as well as provide simultaneous measurements of aerosols that are known to be a major source of error in retrievals of XCO_2 from passive nadir-viewing satellite observations. We show using the global 3-D GEOS-Chem chemistry transport model that a deployment of 50 mini-LHRs to strategically-selected AERONET sites significantly improves our knowledge of global and regional land-based CO_2 fluxes. This improvement varies seasonally and ranges from 58% to 81% over southern lands, 47% to 76% over tropical lands, 71% to 92% over northern lands, and 64% to 91% globally. While column CO_2 measurements from the Total Carbon Column Observing Network (TCCON) provide a similar level of improvement, it is limited to the northern hemisphere where the majority of the 23 TCCON sites are located. We show that supplementing TCCON's existing network with mini-LHR instruments would provide significant improvements in northern hemispheric summertime CO_2 flux estimates which would especially benefit the northernmost latitudes of North America and Eurasia where satellites and ground-based networks have limited data coverage. Our studies suggest that the mini-LHR network could also play a substantive role in reducing carbon flux uncertainty in Arctic and tropical systems by filling in geographical gaps in measurements left by

ground-based networks and space-based observations. A realized network would also provide necessary data for the quinquennial global stocktakes that form part of the Paris Agreement.

1 Introduction

Two recent satellite instruments have made significant contributions to globally characterizing XCO_2: the Japanese Greenhouse gases Observation SATellite (GOSAT) or "IBUKI" launched in 2009 (Kuze et al., 2009), and the Orbiting Carbon Observatory (OCO-2)(Crisp et al., 2017) launched in 2014. The Fourier Transform Spectrometer (FTS) in GOSAT and the grating spectrometer in OCO-2 are both nadir-viewing and observe absorption of XCO_2 using sunlight that has reflected on the Earth's surface, but OCO-2 offers significant improvements in global surface coverage. While GOSAT and OCO-2 have made important advances in observing greenhouse gases from space, poorly characterized systematic errors compromise the accuracy of their data (Wunch et al., 2017) and limit the utility of such datasets for inferring surface flux distributions (Basu et al., 2013). Ground-based networks of accurate/precise XCO2 measurements such as TCCON (Wunch et al., 2017) therefore play an important role in helping to validate these space-borne missions. We describe how we can improve knowledge of the carbon cycle by establishing a network of low-cost, portable mini-LHRs that measure XCO_2, to fill in gaps left by existing column ground-based networks and space-borne observations. These instruments can be quickly deployed (to be collecting data within a few hours) and can run autonomously in the field with little or no maintenance over a period of months or years.

Ground-based, broad spectral column measurements of XCO_2 from the TCCON Fourier Transform Spectrometer (FTS) network have been used to minimize regional systematic errors and serve as a gold standard to validate satellite measurements. In 2010, the TCCON FTS instruments reported a precision limited to ~1 ppm from bias errors due to uncertainties in spectroscopic parameters (Wunch et al., 2010). They resolved this limitation at five of their sites by calibrating their column-averaged dry-air mole fractions to the World Meteorological Organization (WMO) *in situ* trace gas measurements scales using aircraft profiles, and indicated that they planned to eventually perform similar calibrations at the remainder of their sites. While TCCON products are well characterized, the majority of the 23 TCCON sites are in the Northern Hemisphere, leaving important monitoring gaps in regions where our knowledge of the drivers of carbon cycling is uncertain (Shuur et al., 2008;Commane et al., 2017;Saunois et al., 2016;Le Quéré et al., 2016).

The NASA mini-LHRs are designed to be deployed in tandem with AERONET sun photometers (Holben et al., 1998), taking advantage of their sun-trackers. This partnership provides a pathway to establish a global network of mini-LHRs by leveraging AERONET's 500+ site network, and offers a simultaneous measure of aerosol optical depth (AOD) that is a necessary input for satellite retrievals. Because mini-LHRs can collect data during breaks in cloud coverage, this offers the potential for new data products in formerly underrepresented regions such as the Amazon basin, southern Asia monsoon

areas, and the Arctic. These vulnerable geographic regions are not well covered by OCO-2 and GOSAT. Here, using numerical experiments, we simulate a strategic deployment of 50 mini-LHR instruments to AERONET sites and evaluate how this increase in measurement density impacts knowledge of regional and global carbon fluxes.

2 Mini-LHR Instrument Configuration

5 The mini-LHR is a ground-based, passive, sun-viewing instrument that observes trace gases in the atmospheric column. It has been under development at NASA Goddard Space Flight Center (GSFC) since 2009 (Melroy et al., 2015;Clarke et al., 2014;Wilson et al., 2014;Wilson and McLinden, Filed 2012, Issued 2014) and while earlier versions exclusively measured XCO_2, the current version observes both XCO_2 and XCH_4. Current challenges associated with our understanding emissions of CH_4 (Wolf et al., 2017) will result a different network design and therefore will the subject to a future study. The mini-

10 LHR has been tested at altitudes ranging from sea level to 3,400 meters, and in climates that include tropical, subtropical, and temperate zones, extending to just below the Arctic Circle and has shown consistent precisions of 1 ppm XCO_2 and 10 ppb XCH_4 for hourly data products. Fig. 1 shows a mini-LHR monitoring XCO_2 and XCH_4 over thawing permafrost at a remote site in the Bonanza Creek Research Forest near Fairbanks, Alaska. The goal of these field tests was to both improve the quality of the data product as well as test the durability of commercial components that were intended for indoor lab use.

15

The mini-LHR measures XCO_2 by scanning the CO_2 absorption feature near 1.61 μm. Fig. 2 shows the current configuration of the system and Table 1 lists key system parameters. Sunlight is collected with a fibre-coupled, 0.2-degree field-of-view collimator that is non-invasively connected to an AERONET sun tracker. Once collected, sunlight is modulated with a fibre switch, superimposed with infrared laser light from a distributive feedback laser in a single mode fibre coupler, and then

20 mixed in a fast photoreceiver/InGaAs detector to produce an RF beat signal. The RF receiver separates RF and DC outputs, and the RF signal is amplified, filtered, and then detected with a square-law detector. The resulting signal is measured with a lock-in amplifier referenced to the fibre switch frequency as the laser scans across an absorption feature. A microprocessor controls the laser scanning and data collection. The mini-LHR has spectral sampling resolution of ~ 0.013 cm^{-1} which is 15 times higher than GOSAT (~ 0.2 cm^{-1}), 20 times higher than OCO-2 (~ 0.3 cm^{-1}) and slightly higher than TCCON (~ 0.02

25 cm^{-1}). Individual scans of the CO_2 feature are collected at 2 minute intervals throughout the day during sunlight hours when clouds are not present and averaged into hourly data products.

3 Data Processing and Retrieval

Averaged absorption scans are analyzed to extract column mole fractions of CO_2 using custom analysis software developed at GSFC that is similar to the approach used by TCCON. There are two main steps involved in processing data: (1)

simulating the spectra (mathematically simulating what the mini-LHR observes in the atmosphere), and (2) fitting the simulation to the data to extract the abundance of XCO_2.

We simulate the spectra using the Planetary Spectrum Generator (PSG), which is an online tool developed at NASA GSFC
5 (Villanueva et al., 2016;Villanueva et al., 2015) for synthesizing Earth and planetary spectra (atmospheres and surfaces) for a broad range of wavelengths (0.1 μm to 100 mm, UV/Vis/near-IR/IR/far-IR/THz/sub-mm/Radio) from any observatory, orbiter, or lander. This is achieved by combining several state-of-the-art radiative transfer models, spectroscopic databases and planetary databases. The PSG code includes refraction of sunlight through the atmosphere as well as a computationally efficient scattering package that incorporates the latest radiative transfer numerical methods (Villanueva et al., 2015;Smith et
10 al., 2009), and is parameterized for LTE (Local-Thermodynamic Equilibrium) calculations. The PSG is operated remotely by employing a versatile online Application Program Interface (API). The API operates by sending a configuration file to the PSG servers. Upon reception of the configuration file, PSG computes and returns the spectra.

Part of this simulation includes the Modern-Era Retrospective analysis for Research and Applications, Version 2 (MERRA-
15 2) data set which provides meteorological inputs (Reichle et al., 2011;Rienecker, 2011) and provides a $N_L = 72$ layer model of the atmosphere. Our code computes temperature (T) and pressure (P) abundances for Earth by first selecting a set of 6 standard profiles based on season and latitude: Tropical', 'Midlatitude-Summer', 'Midlatitude-Winter', 'Subarctic-Summer', 'Subarctic-Winter', 'US-Standard' (Anderson et al., 1986). These profiles provide abundances for a myriad of species and basic temperature and pressure profiles. The code then extracts P, T, O_3, H_2O and water ice abundances from the MERRA
20 database for this location and time. The MERRA-2 grid is described on a coarse grid and it does not contain fine elevation information and therefore the GTOPO30 topography database (~1 km resolution) is also used to derive the exact elevation of the mini-LHR site location. The information from MERRA-2 lat/lon is then refined in elevation (using scaleheights, etc.) using this high-resolution map.

25 Our code generates an initial configuration file that establishes the location and date/time of the measurement. Using this configuration file, the code calls the PSG/API and this returns all of the geometry parameters (air mass, phase angle, etc.) and an *a priori* vertical profile based on the date and location. Then, using this configuration file, the program goes into the fitting routine that calls the PSG/API to get calculate spectra by fitting the CO_2 abundance. The fit perturbs the CO_2 abundance and obtains a fit based on the Levenberg-Marquardt algorithm which is an iterative least-squares curve fitting
30 procedure.

3.1 Instrument Calibrations, Validations, and Establishment of Errors and Uncertainties

Mini-LHR instruments periodically undergo a calibration/validation procedure at NASA GSFC to track performance and establish documented traceability of column data products. In particular, we calculate and report measurement precision,

measurement error, and measurement bias, as defined by the Vocabulaire International de Metrologie (VIM) (Meaures, 2012).

We estimate measurement precision (standard deviation) by routine laboratory calibrations. In the calibration procedure, the
5   mini-LHR instrument scans a NIST (National Institute of Standards and Technology) traceable atmospheric mixture of gases (NIST Traceable Reference Material Program for Gas Standards, 2016) in a 36-meter Herriot absorption cell. The NIST traceable atmospheric mixture of gases fulfils the criteria of a measurement standard with a negligible measurement uncertainty. The calibration gas standards are specified in the Code of Federal Regulations (CFR) to calibrate instruments used to monitor regulated emissions. The standard deviation of the points in the scan provides an estimate of precision while
10   regular calibrations track any measurement bias (systematic measurement error).

In ongoing work, we are also estimating measurement error with a side-by-side comparison of column data products from the mini-LHR and the TCCON FTS located at NASA Armstrong Flight Research Center (AFRC) at Moffett Field, CA. The TCCON FTS measures column CH_4 and CO_2 at the same wavelengths but at lower resolution than the mini-LHR. While
15   TCCON has a well-documented history of characterization, we refer to this as an "estimate" of measurement error due to differences in resolution and because there are known biases between TCCON sites (1% for CO_2 at US sites and 1.1% $\pm$ 0.2% at European sites) (Wunch et al., 2010).

For passive satellite observations, scattering from clouds and aerosols are known to be significant source of retrieval error
20   for XCO_2 (Mao and Kawa, 2004;Aben et al., 2007;Uchino et al., 2012;Yoshida et al., 2013). This is primarily because these are nadir-pointing instruments that view sunlight reflected on a portion of ground that is illuminated by direct sunlight as well as scattered sunlight from clouds and aerosols. In contrast, ground-passive measurements have a narrow field-of-view (FOV) and point directly at the sun. The TCCON at Park Falls, WI for example, has a FOV of ~0.14 degrees and mini-LHRs have a FOV of ~0.2 degrees (compared to the sun which has a field of view of ~0.5 degrees). Because the FOVs of
25   these instruments are narrower than that of the sun, their light collection optics do not accept the scattered light outside of this FOV. Consequently, the mini-LHR and TCCON are mainly impacted by extinction, resulting in lower levels of sunlight reaching these ground instruments and lower signal-to-noise levels. Solar intensity variations that impact TCCON are corrected by dividing the interferograms by the unmodulated DC signal (Wunch et al., 2011). For the mini-LHR, transmittance scans are corrected for extinction by dividing scans by a fitted baseline that tracks fluctuations in solar
30   irradiance.

4 Theoretical Potential of Network to Improve Knowledge of Regional Carbon Fluxes

We use numerical experiments to provide an upper limit on the theoretical potential of the proposed network on reducing the uncertainty of regional carbon flux estimates. The approach we take is to define a closed-loop experiment, often called Observing System Simulation Experiments (OSSEs), in which we define the true atmospheric state using a global 3-D model of atmospheric chemistry and transport driven by true surface fluxes. This true atmospheric state is then sampled, as it would be by the mini-LHRs (e.g. time, location and vertical sensitivity). We then generate a complementary set of model values that are generated from an independent surface flux inventory, including differences in the magnitude and distribution of fluxes; we use this independent inventory as our *a priori* for the OSSEs. We infer the *a posteriori* fluxes from measurements using an ensemble Kalman Filter.

We use v9.02 of the GEOS-Chem model of atmospheric chemistry and transport (http://geos-chem.org) driven by GEOS-5 analysed meteorological fields that includes a simulation of atmospheric CO_2 that has been evaluated with a range of ground-based, aircraft and satellite observations (Feng et al., 2011;Feng et al., 2009;Feng et al., 2016). For our experiments, we use the model at a horizontal resolution of 4º latitude x 5º longitude for an arbitrary year, which in our experiments is 2009. We use monthly ODIAC fossil fuel emissions (Oda and Maksyutov, 2011), monthly ocean biosphere fluxes (Takahashi et al., 2009), and weekly biomass burning emissions from GFEDv3 (van der Werf et al., 2010).

Currently, it is common practice to assume that most of the uncertainty in atmospheric CO_2 stems from natural fluxes so other sources are typically assumed to be well described by existing inventories (e.g. Gurney et al, 2008). While this practice is slowly being challenged by the community we retain these assumption for the purpose of our theoretical calculations. To define our true atmospheric state we use three-hourly land biosphere fluxes from the ORCHIDEE land surface model (Krinner et al, 2005) and in a separate model calculation to define our *a priori* state we use three-hourly land biosphere fluxes from CASA (Olsen and Randerson, 2004). Fig. 4 shows there are significant differences in the magnitudes and distributions of ORCHIDEE and CASA land biosphere CO_2 fluxes so that our OSSE provides a rigorous test of the theoretical data.

Our retrieval simulation requires a matrix of averaging kernels (**A**) that describe the sensitivity of the retrieved state vector $\hat{x}$ (in this case, a vector describing the vertical profile of CO_2 described over n atmospheric layers) to the "true" state vector x, for different values of solar zenith angle throughout the day. Using the standard convention, upper case and lower case emboldened variables denote a matrix and vector, respectively, and superscripts -1 and T denote matrix inverse and transpose operations, respectively. The averaging kernel is calculated as (Rodgers, 2000;Liuzzi et al., 2016):

$$\mathbf{A} = \frac{\partial \hat{x}}{\partial x} = (\mathbf{S}_a^{-1} + \mathbf{K}^T \mathbf{S}_\epsilon^{-1} \mathbf{K})^{-1} \mathbf{K}^T \mathbf{S}_\epsilon^{-1} \mathbf{K}, \qquad (1)$$

where $\mathbf{S}_a$ is the *a priori* error covariance matrix (size n x n); $\mathbf{S}_\epsilon$ is the measurement error covariance matrix (size m x m, where m denotes the length of the radiance vector); and $\mathbf{K}$ is the matrix of weighting functions describes the derivative of the radiance with respect to a change in the CO_2 profile (size m x n). The matrix of averaging kernel is used here to describe the instrument sensitivity to changes in CO_2 so we can simulate mini-LHR XCO2 column measurements in GEOS-Chem. For simplicity, we assume $\mathbf{S}_a$ and $\mathbf{S}_\epsilon$ are diagonal and represent the square of the background variability of CO_2 concentration in each atmospheric layer and the square of the instrument noise, respectively.

The sum of the rows of $\mathbf{A}$ corresponds to summing the retrieval sensitivities to the CO_2 in each atmosphere layer, and describe the sensitivity of the atmospheric column to a change in atmospheric CO_2 in the vertical profile, i.e. the column averaging kernel $\mathbf{a}$. In the ideal case, each summed row would be close to unity. Fig. 3 shows that for a variety of solar zenith angles, a > 0.8 in the troposphere but falls off quickly in the stratosphere, consistent with TCCON averaging kernels (Wunch et al., 2011).

We also calculate the number of Degrees of Freedom (DOF) of the retrieval as the trace of $\mathbf{A}$, which estimates the number of independent pieces of information that can be derived from retrieval. In the case of the column XCO_2 retrieval, this should be close to or higher than 1; values less than one indicate the influence of *a priori* information (Camy-Peyret et al., 2017). We find that with a SNR value of 500 and an assumed *a priori* variance of 5% for CO_2 concentrations results in a DOF between 0.88 and 2.10.

To infer regional fluxes of CO_2 from the measurements, we use an established ensemble Kalman Filter approach (Feng et al., 2009;Feng et al., 2016;Feng et al., 2017). For brevity, we refer the reader to Feng et al 2009 for a detailed description of the approach and its application within GEOS-Chem. We adopt a uniform 50% *a priori* uncertainty and assume 1.5 ppm for individual measurement and model transport errors. To characterize the impact of the mini-LHR measurements on the *a priori* knowledge we use a metric that describes how uncertainty of fluxes have reduced after the *a priori* has been informed by the measurements: $\gamma = 1 - \mathbf{S}_c^{ii}/\mathbf{S}_d^{ii}$, where $\mathbf{S}_c^{ii}$ and $\mathbf{S}_d^{ii}$ denote the diagonal elements of the *a posteriori* and *a priori* CO_2 flux error covariance matrices, respectively. A larger value for γ denotes a larger scientific impact of the observations. We also report comparisons between true, *a priori*, and *a posteriori* CO_2 fluxes over key geographical regions. Together, our use of two independent land biosphere flux inventories, the γ metric and the inter-comparison of fluxes provide a transparent theoretical assessment of the LHR data to quantify geographical fluxes of CO_2.

We performed three experiments to estimate true CO_2 fluxes: 1) using TCCON measurements with their current measurement configuration (Fig. 4); 2) using mini-LHR measurements collected at the TCCON measurement sites; and 3) using mini-LHR measurements collected an enhanced measurement configuration. We conservatively assume a mini-LHR

Atmospheric
Measurement
Techniques
Discussions

measurement precision of 1.5 ppm in our experiments, however, the current precisions for the mini-LHR and TCCON data products are <1 ppm for one-hour data products (Wunch et al., 2010;Messerschmidt et al., 2011;Wilson et al., 2017;Melroy et al., 2015). Instrument biases were not included in these OSSE runs.

5   Table 2 lists the proposed enhanced distribution of mini-LHR instruments. These sites were initially chosen to target regions where AERONET sites already existed and where there are gaps in the existing *in situ* measurements, TCCON measurements, and satellite observations. Consideration was also given to accessibility, acknowledging evolving political environments. Consequently, the enhanced network has not been optimized in any way.

10   Performance of the mini-LHR instruments (not shown) distributed using the current TCCON measurement configuration is comparable with the TCCON instruments (Fig. 5), despite larger assumed random errors. We find this is primarily due to the relatively comparable role of instrument error compared to atmospheric transport model errors (1.5 ppm) particularly at the 4° latitude x 5° longitude horizontal resolution employed here. Using finer-scale meteorology could very well reduce model error but knowledge of this error is poorly defined with no robust quantitative method currently available. Fig. 5 and 6

15   provide an overview of the agreement between true and *a posteriori* CO_2 fluxes inferred from TCCON data. As expected, TCCON can broadly reproduce true fluxes but the current TCCON configuration is insensitive to some geographical regions (e.g. North Africa) thereby limiting our ability to study systematic biases in the satellite data over this region.

     Fig. 7 shows that the mini-LHR enhanced network of 50 sites results in global and significant improvements in our

20   knowledge of CO_2 fluxes. Table 3 shows error reductions (γ) over integrated large-scale regions for winter and summer months as well as median values. Significant values of the γ are found over most of North America and Eurasia although significant improvements are also found over South America and southern Africa. There is a similar geographical distribution of improvements during boreal summer months but with larger values over North America and Eurasia including the northernmost latitudes. Similar calculations for the TCCON network shows comparable levels of improvement but are

25   more spatially limited, particularly over the northern hemisphere. We find that, as expected, the elevated mini-LHR network outperforms the TCCON network by virtue of our network design (i.e. number and location of mini-LHR sensors) with closer agreement with true fluxes (Fig. 5) and smaller root-mean-square errors over major ecosystems (Fig. 6).

     The mobility of mini-LHR sensors, allows us to locate them in remote environments where an AERONET site is already

30   established. This includes in particular tropical ecosystems, where the physical environment is challenging for large-scale instrument installations, and at polar latitudes where space-borne measurements are compromised because of low solar illumination and low surface reflectance over snow/ice. This suggests that the mini-LHR network could play a substantive role in an Arctic monitoring network, particularly during spring and autumn months.

Atmospheric
Measurement
Techniques
Discussions

Open Access

EGU

Fig. 7 also demonstrates the complementarity of the mini-LHR and TCCON networks. Inter-calibrating sensors from both networks theoretically represent observational constraints on CO_2 fluxes that rival knowledge inferred from *in situ* observation network over some land masses (*e.g.*, North America and Eurasia), and outperform on other land masses (*e.g.*, tropics). The *in situ* networks provide an invaluable record on the changing carbon cycle by putting present-day changes in

5   an historical context, whose value is reduced if they are terminated.

5 Conclusion

With a modest deployment of mini-LHR instruments to 50 sites, numerical experiments with the GEOS-Chem model indicate that the resulting XCO_2 data products lead to improvements of carbon flux uncertainties ranging from 58% to 81% over southern lands, 47% to 76% over tropical lands, 71% to 92% over northern lands, and 64% to 91% globally. Because

10   mini-LHRs leverage AERONET's global network of more than 500 sites worldwide, additional instruments can be rapidly added to target specific areas of uncertainty such as thawing permafrost emissions in the Arctic or tropical ecosystems in the mid-latitudes. In addition to infrastructure, co-location of these instruments provides a simultaneous measurement of aerosol optical depth which is necessary to evaluate and correct aerosol scattering effects in XCO_2 satellite retrievals and consequent uncertainty in local and regional carbon flux estimates. Sun-viewing mini-LHR instruments are not impacted by some of the

15   issues that degrade the quality of airborne or space-borne techniques that use reflected sunlight: surface reflectivity (e.g., darkness and angular dependence), surface roughness (sunlight path-length), geo-location error, and aerosol /cloud scattering. Together with the capability of measuring through gaps in cloud cover and continuous observation during daylight hours, the mini-LHR surface network in tandem operation with AERONET could provide full global and seasonal observation coverage and offer a necessary validation product for orbital missions.

References

Aben, I., Hasekamp, O., and Hartmann, W.: Uncertainties in the space-based measurements Of CO2 columns due to scattering in the Earth's atmosphere, J. Quant. Spectros. Radiat. Transfer, 104, 450-459, 10.1016/j.jqsrt.2006.09.013, 2007.

Anderson, G. P., Chetwynd, J. H., Clough, S. A., Shettle, E. P., and Kneizys, F. X.: AFGL Atmospheric Constituent Profiles (0-120km), Air Force Geophysics Laboratory, Hanscom AFB, MA 01731AD-A175 173, 43, 1986.

Basu, S., Guerlet, S., Butz, A., Houweling, S., Hasekamp, O., Aben, I., Krummel, P., Steele, P., Langenfelds, R. L., Torn, M., Biraud, S. C., Stephens, B. B., Andrews, A., and Worthy, D.: Global CO2 fluxes estimated from GOSAT retrievals of total column CO2, Atmos.

5   Chem. Phys., 13, 8695-8717, 10.5194/acp-13-8695-2013, 2013.

Camy-Peyret, C., Liuzzi, G., Masiello, G., Serio, C., Venafra, S., and Montzka, S.: Assessment of IASI capability for retrieving carbonyl sulphide (OCS), J. Quant. Spect. Rad. Trans., 201, 197-208, 10.1016/j.jqsrt.2017.07.006, 2017.

Clarke, G. B., Wilson, E. L., Miller, J. H., and Melroy, H. R.: Uncertainty analysis for the miniaturized laser heterodyne radiometer (mini-LHR), Measurement Science and Technology, 25, 055204-055209, 10.1088/0957-0233/25/5/055204, 2014.

10   Commane, R., Lindaas, J., Benmergui, J., Luus, K. A., Change, R. Y.-W., Daube, B. C., Euskirchen, E. S., Henderson, J. M., Kariong, A., Miller, J. B., Miller, S. M., Parazoo, N. C., Randerson, J. T., Sweeney, C., Tans, P., Thoning, K., Veraverbeke, S., Miller, C. E., and Wofsy, S. C.: Carbon dioxide sources from Alaska driven by increasing early winter respiration from Arctic tundra, Proceedings of the National Academy of Sciences of the United States of America (PNAS), 114, 5361-5366, 10.1073/pnas.1618567114, 2017.

Crisp, D., Pollock, H. R., Rosenberg, R., Chapsky, L., Lee, R. A. M., Oyafuso, F. A., Frankenberg, C., O'Dell, C. W., Bruegge, C. J.,

15   Doran, G. B., Eldering, A., Fisher, B. M., Fu, D., Gunson, M. R., Mandrake, L., Osterman, G. B., Schwandner, F. M., Sun, K., Taylor, T. E., Wennberg, P. O., and Wunch, D.: The on-orbit performance of the Orbiting Carbon Observatory-2 (OCO-2) instrument and its radiometrically calibrated products, Atmos. Meas. Tech., 10, 59-81, 10.5194/amt-10-59-2017, 2017.

Feng, L., Palmer, P., Bosch, H., and Dance, S.: Estimating surface CO2 fluxes from space-borne CO2 dry air mole fraction observations using an ensemble Kalman Filter, Atmos. Chem. Phys., 9, 2619-2633, 10.5194/acp-9-2619-2009, 2009.

20   Feng, L., Palmer, P., Yang, Y., Yantosca, R. M., Kawa, S. R., Paris, J.-D., Matsueda, H., and Machida, T.: Evaluating a 3-D transport model of atmospheric CO2 using ground-based, aircraft, and space-borne data, Atmos. Chem. Phys., 11, 2789–2803, 2011.

Feng, L., Palmer, P. I., Parker, R. J., Deutscher, N. M., Feist, D. G., Kivi, R., Morino, I., and Sussmann, R.: Estimates of European uptake of CO2 inferred from GOSAT XCO2 retrievals: sensitivity to measurement bias inside and outside Europe, Atmos. Chem. Phys., 16, 1289-1302, 10.5194/acp-16-1289-2016, 2016.

25   Feng, L., Palmer, P. I., Bösch, H., Parker, R. J., Webb, A. J., Correia, C. S. C., Deutscher, N. M., Domingues, L. G., Feist, D. G., Gatti, L. V., Gloor, E., Hase, F., Kivi, R., Liu, Y., Miller, J. B., Morino, I., Sussmann, R., Strong, K., Uchino, O., Wang, J., and Zahn, A.: Consistent regional fluxes of CH4 and CO2 inferred from GOSAT proxy XCH4 : XCO2 retrievals, 2010–2014, Atmos. Chem. Phys., 17, 4781-4797, 10.5194/acp-17-4781-2017, 2017.

Holben, B. N., Eck, T. F., Slutsker, I., Tanre, D., Buis, J. P., Setzer, A., Vermote, E., Reagan, J. A., Kaufman, Y. J., Nakajima, T.,

30   Lavenue, F., Jankowiak, I., and Smirnov, A.: AERONET - A federated instrument network and data archive for aerosol characterization, Remote Sensing of Environment, 66, 1-16, 1998.

Kuze, A., Suto, H., Nakajima, H., and Hamazaki, T.: Thermal and near infrared sensor for carbon observation Fourier-transform spectrometer on the greenhouse gases observing satellite for greenhouse gases monitoring, Applied Optics, 48, 6716-6733, 2009.

Le Quéré, C., Andrew, R. M., Canadell, J. G., Sitch, S., Korsbakken, J. I., Peters, G. P., Manning, A. C., Boden, T. A., Tans, P. P.,

35   Houghton, R. A., Keeling, R. F., Alin, S., Andrews, O. D., Anthoni, P., Barbero, L., Bopp, L., Chevallier, F., Chini, L. P., Ciais, P., Currie, K., Delire, C., Doney, S. C., Friedlingstein, P., Gkritzalis, T., Harris, I., Hauck, J., Haverd, V., Hoppema, M., Klein Goldewijk, K., Jain, A. K., Kato, E., Körtzinger, A., Landschützer, P., Lefèvre, N., Lenton, A., Lienert, S., Lombardozzi, D., Melton, J. R., Metzl, N., Millero, F., Monteiro, P. M. S., Munro, D. R., Nabel, J. E. M. S., Nakaoka, S. I., O'Brien, K., Olsen, A., Omar, A. M., Ono, T., Pierrot, D., Poulter, B., Rödenbeck, C., Salisbury, J., Schuster, U., Schwinger, J., Séférian, R., Skjelvan, I., Stocker, B. D., Sutton, A. J., Takahashi, T., Tian, H.,

40   Tilbrook, B., van der Laan-Luijkx, I. T., van der Werf, G. R., Viovy, N., Walker, A. P., Wiltshire, A. J., and Zaehle, S.: Global Carbon Budget 2016, Earth Syst. Sci. Data, 8, 605-649, 10.5194/essd-8-605-2016, 2016.

Liuzzi, G., Masiello, G., Serio, C., Venafra, S., and Camy-Peyret, C.: Physical inversion of the full IASI spectra: Assessment of atmospheric parameters retrievals, consistency of spectroscopy and forward modelling, Journal of Quantitative Spectroscopy and Radiative Transfer, 182, 128-157, https://doi.org/10.1016/j.jqsrt.2016.05.022, 2016.

45   Mao, J.-P., and Kawa, S. R.: Sensitivity studies for space-based measurement of atmospheric total column carbon dioxide by reflected sunlight, Applied Optics, 43, 914-927, 2004.

Meaures, B. I. d. p. e.: JCM 200:1012: International vocabulary of metrology - Basic and general concepts and associated terms (VIM), 3rd edition, http://www.bipm.org/en/publications/guides/vim.html, 108 pages, 2012.

Melroy, H. R., Wilson, E. L., Clarke, G. B., Ott, L. E., Mao, J.-P., Ramanathan, A. K., and McLinden, M. L.: Autonomous field

50   measurements of CO2 in the atmospheric column with the miniaturized laser heterodyne radiometer (Mini-LHR), Applied Physics B, 120, 609-615, 2015.

Messerschmidt, J., Geibel, M. C., Blumenstock, T., Chen, H., Deutscher, N. M., Engel, A., Feist, D. G., Gerbig, C., Gisi, M., Hase, F., Katrynski, K., Kolle, O., Lavric, J. V., Notholt, J., Palm, M., Ramonet, M., Rettinger, M., Schmidt, M., Sussmann, R., Toon, G. C., Truong, F., Warneke, T., Wennberg, P. O., Wunch, D., and Xueref-Remy, I.: Calibration of TCCON column-averaged CO2: the first

55   aircraft campaign over European TCCON sites, Atmos. Chem. Phys., 11, 10765-10777, 10.5194/acp-11-10765-2011, 2011.

Oda, T., and Maksyutov, S.: A very high-resolution (1 km×1 km) global fossil fuel CO_2 emission inventory derived using a point source database and satellite observations of nighttime lights, Atmos. Chem. Phys., 11, 543-556, 10.5194/acp-11-543-2011, 2011.

Olsen, S. C., and Randerson, J. T.: Differences between surface and column atmospheric CO2 and implications for carbon cycle research, Journal of Geophysical Research: Atmospheres, 109, n/a-n/a, 10.1029/2003JD003968, 2004.

5   Reichle, R. H., Koster, R. D., DeLannoy, G. J. M., Forman, B. A., Liu, Q., Mahanama, S. P. P., and Toure, A.: Assessment and Enhancement of MERRA Land Surface Hydrology Estimates, J. Climate, 24, 6322-6338, 2011.

Rienecker, M. M., et al.: MERRA: NASA's Modern-Era Retrospective Analysis for Research and Applications, J. Climate, 24, 3624-3648, 2011.

Rodgers, C. D.: Inverse Methods for Atmospheric Sounding, Theory and Practice, Series of Atmospheric Oceanic and Planetary Physics,
10 Series on Atmospheric, Oceanic, and Planetary Physics, Oxford Press, 2000.

Saunois, M., Bousquet, P., Poulter, B., Peregon, A., Ciais, P., Canadell, J. G., Dlugokencky, E. J., Etiope, G., Bastviken, D., Houweling, S., Janssens-Maenhout, G., Tubiello, F. N., Castaldi, S., Jackson, R. B., Alexe, M., Arora, V. K., Beerling, D. J., Bergamaschi, P., Blake, D. R., Brailsford, G., Brovkin, V., Bruhwiler, L., Crevoisier, C., Crill, P., Covey, K., Curry, C., Frankenberg, C., Gedney, N., Höglund-Isaksson, L., Ishizawa, M., Ito, A., Joos, F., Kim, H. S., Kleinen, T., Krummel, P., Lamarque, J. F., Langenfelds, R., Locatelli, R.,
15 Machida, T., Maksyutov, S., McDonald, K. C., Marshall, J., Melton, J. R., Morino, I., Naik, V., O'Doherty, S., Parmentier, F. J. W., Patra, P. K., Peng, C., Peng, S., Peters, G. P., Pison, I., Prigent, C., Prinn, R., Ramonet, M., Riley, W. J., Saito, M., Santini, M., Schroeder, R., Simpson, I. J., Spahni, R., Steele, P., Takizawa, A., Thornton, B. F., Tian, H., Tohjima, Y., Viovy, N., Voulgarakis, A., van Weele, M., van der Werf, G. R., Weiss, R., Wiedinmyer, C., Wilton, D. J., Wiltshire, A., Worthy, D., Wunch, D., Xu, X., Yoshida, Y., Zhang, B., Zhang, Z., and Zhu, Q.: The global methane budget 2000–2012, Earth Syst. Sci. Data, 8, 697-751, 10.5194/essd-8-697-2016, 2016.

20 Shuur, E. A. G., Bockheim, J., Canadell, J. G., Euskirchen, E., Field, C. B., Goryachkin, S. V., Hagemann, S., Kuhry, P., Lafleur, P. M., Lee, H., Mazhitova, G., Nelson, F. E., Rinke, A., Romanovsky, V. E., Shiklomanov, N., Tarnocai, C., Venevsky, S., Vogel, J. G., and Zimov, S. A.: Vulnerability of permafrost carbon to climate change: Implications for the global carbon cycle, Bioscience, 58, 701-714, 10.1641/B580807, 2008.

Smith, M. D., Wolff, M. J., Clancy, R. T., and Murchie, S. L.: Compact Reconnaissance Imaging Spectrometer observations of water
25 vapor and carbon monoxide, J. Geophys. Res., 114, 10.1029/2008JE003288, 2009.

Takahashi, T., Sutherland, S. C., Wanninkhof, R., Sweeney, C., Feely, R. A., Chipman, D. W., Hales, B., Friederich, G., Chavez, F., Sabine, C., Watson, A., Bakker, D. C. E., Schuster, U., Metzl, N., Yoshikawa-Inoue, H., Ishii, M., Midorikawa, T., Nojiri, Y., Kortzinger, A., Steinhoff, T., Hoppema, M., Olafsson, J., Arnarson, T. S., Tilbrook, B., Johannessen, T., Olsen, A., Bellerby, R., Wong, C. S., Delille, B., Bates, N. R., and de Baar, H. J. W.: Climatological mean and decadal changes in surface ocean pCO2, and net sea-air CO2 flux over
30 the global oceans, Deep Sea Res. Part II, 56, 554–577, doi:10.1016/j.dsr2.2008.12.009, 2009.

Uchino, O., Kikuchi, N., Sakai, T., Morino, I., Yoshida, Y., Nagai, T., Shimizu, A., Shibata, T., Yamazaki, A., Uchiyama, A., Kikuchi, N., Oshchepkov, S., Bril, A., and Yokota, T.: Influence of aerosols and thin cirrus clouds on the GOSAT-observed CO2: a case study over Tsukuba, Atmos. Chem. Phys., 12, 3393-3404, 10.5194/acp-12-3393-2012, 2012.

van der Werf, G. R., Randerson, J. T., Giglio, L., Collatz, G. J., Mu, M., Kasibhatla, P. S., Morton, D. C., DeFries, R. S., Jin, Y., and van
35 Leeuwen, T. T.: Global fire emissions and the contribution of deforestation, savanna, forest, agricultural, and peat fires (1997–2009), Atmos. Chem. Phys., 10, 11707-11735, 10.5194/acp-10-11707-2010, 2010.

Villanueva, G. L., Mumma, M. J., Novak, R. E., Kaufl, H. U., Hartogh, P., Encrenaz, T., Tokunaga, A., Khayat, A., and Smith, M. D.: Strong water isotopic anomalies in the martian atmosphere: Probing current and ancient reservoirs, Science, 348, 218-221, 2015.

Villanueva, G. L., Smith, M., Wolff, M. J., Protopapa, S., Hewagama, T., Mandell, A. M., and Faggi, S.: Planetary Spectrum Generator
40 (PSG). Retrieved from https://ssed.gsfc.nasa.gov/psg/about.html, 2016.

Wilson, E. L., McLinden, M. L., Miller, J. H., Allen, G. R., Ott, L. E., Melroy, H. R., and Clarke, G. B.: Miniaturized Laser Heterodyne Radiometer for Measurements of CO2 in the Atmospheric Column, Applied Physics B: Lasers & Optics, 114, 385-393, 10.1007/s00340-013-5531-1, 2014.

Wilson, E. L., DiGregorio, A. J., Riot, V. J., Ammons, M. S., Bruner, W. W., Carter, D., Mao, J.-P., Ramanathan, A., Strahan, S. E.,
45 Oman, L. D., Hoffman, C., and Garner, R. M.: A 4 U laser heterodyne radiometer for methane (CH4) and carbon dioxide (CO2) measurements from an occultation-viewing CubeSat, Measurement Science and Technology, 28, 035902, 10.1088/1361-6501/aa5440, 2017.

Wolf, J., Asrar, G. R., and West, T. O.: Revised methane emissions factors and spatially distributed annual carbon fluxes for global livestock, Carbon Balance and Management, 12, 16, 10.1186/s13021-017-0084-y, 2017.

50 Wunch, D., Toon, G. C., Wennberg, P. O., Wofsy, S. C., Stephen, M., Fischer, M. L., Uchino, O., Abshire, J. B., Bernath, P. F., Biraud, S. C., Blavier, -. F., L., Boone, C., Bowman, K. P., Browell, E. V., Campos, T., Connor, B. J., Daube, B. C., Deutscher, N. M., Diao, M., Elkins, J. W., Gerbig, C., Gottlieb, E., Griffith, D., Hurst, D. F., Jimenez, R., Keppel-Aleks, G., Kort, E. A. I., Park, S., Robinson, J., Roehl, C. M., Sawa, Y., Sherlock, V., Sweeney, C., Tanaka, T., and Zondo, M. A.: Calibration of the Total Carbon Column Observing Network using aircraft profile data, Atmos. Meas. Tech., 3, 1351-1362, 10.5194/amt-3-1351-2010, 2010.

Wunch, D., Toon, G. C., Blavier, -. F., L., Washenfelder, R. A., Notholt, J., Connor, B., Griffith, D. W. T., Sherlock, V., and Wennberg, P. O.: The total carbon column observing network (TCCON), Philosophical Transactions of the Royal Society a-Mathematical Physical and Engineering Sciences, 369, 2087-2112, 2011.

Wunch, D., Wennberg, P. O., Osterman, G., Fisher, B., Naylor, B., Roehl, C. M., O'Dell, C., Mandrake, L., Viatte, C., Kiel, M., Griffith,

5   D. W. T., Deutscher, N. M., Velazco, V. A., Notholt, J., Warneke, T., Petri, C., De Maziere, M., Sha, M. K., Sussmann, R., Rettinger, M., Pollard, D., Robinson, J., Morino, I., Uchino, O., Hase, F., Blumenstock, T., Feist, D. G., Arnold, S. G., Strong, K., Mendonca, J., Kivi, R., Heikkinen, P., Iraci, L., Podolske, J., Hillyard, P. W., Kawakami, S., Dubey, M. K., Parker, H. A., Sepulveda, E., García, O. E., Te, Y., Jeseck, P., Gunson, M. R., Crisp, D., and Eldering, A.: Comparisons of the Orbiting Carbon Observatory-2 (OCO-2) XCO2 measurements with TCCON, Atmos. Meas. Tech., 10, 2209-2238, 10.5194/amt-10-2209-2017, 2017.

10   Yoshida, Y., Kikuchi, N., Morino, I., Uchino, O., Oshchepkov, S., Bril, A., Saeki, T., Schutgens, N., Toon, G. C., Wunch, D., Roehl, C. M., Wennberg, P. O., Griffith, D. W. T., Deutscher, N. M., Warneke, T., Notholt, J., Robinson, J., Sherlock, J., Connor, B., Rettinger, M., Sussmann, R., Ahonen, P., Heikkinen, P., Kyro, E., Mendonca, J., Strong, K., Hase, F., Dohe, S., and Yokota, T.: Improvement of the retrieval algorithm for GOSAT SWIR XCO2 and XCH4 and their validation using TCCON data, Atmos. Meas. Tech., 6, 1533-1547, 10.5194/amt-6-1533-2013, 2013.

15

Atmospheric
Measurement
Techniques
Discussions

Table 1: Averaging kernels for the mini-LHR were calculated for the Bonanza Creek site using parameters in the table that follows. The molecules analyzed in the 72 layer atmosphere included 1:H_2O, 2:CO_2, 3:O_3, 4:N_2O, 5:CO, 6:CH_4, 7:O_2, 8:N_2 and the level of variability was 0.05 (where 1:100% variability, 0:no-variability).

Parameter	Value	Units
Instrument lower wavelength	1.61137	μm
Instrument upper wavelength	1.641165	μm
Instrument resolution at FWHM	0.000003	μm
Instrument's data SNR	500	d
a-priori variance	5	%
Zenith angle range	0-60	deg
Latitude	64 + 42.055/60.0	N degrees
Longitude	360 - (148 + 18.763/60.0)	E degrees
UT date/time of observations to extract MERRA values	'2016/05/30 19:15'	yyyy/mm/dd hh:mm

5

Table 2: List of 50 selected AERONET sites with mini-LHR installed in the future for the OSSE study.

Site	Latitude	Longitude	Site	Latitude	Longitude
Edinburgh, UK	55.9	-3.2	Birdsville, Australia	-25.88	139.33
NASA/GSFC, MD, USA	39.0	-76.9	Bribane, Australia	-27.50	153.00
Park Falls, WI, USA	45.9	-90.3	Lake_lefroy, Australia	-31.25	121.70
Mauna Loa, HI, USA	19.5	-155.6	Gobabeb, Namibia	-23.55	15.03
Tamanrasset, Algeria	22.8	5.5	WITS, South Africa	-26.20	28.01
Fairbanks, Alaska, USA	64.8	-147.7	SEGC, Africa	-0.20	11.60
Yellowknife, Canada	62.4	-114.4	Santiago, Chile	-33.50	-70.60
Yakutsk, Russia	62.0	129.7	Rio_de_Janeiro_UFRJ, Brazil	-22.83	-43.25
Red Mountain Pass, CO, USA	37.9	-107.7	CEILAP-BA, Argentina	-34.58	-58.50
Manaus, Brazil	-3.2	-60.0	Arica, Chile	-18.49	-70.30
Rio Franco, Brazil	10.0	-67.9	Churchhill, Canada	58.73	-93.83
Pretoria, South Africa	25.8	28.2	Kelowna, Canada	49.92	-119.40
Kibale, Uganda	0.5	30.4	Ittoqqortoormiit, Greenland	70.50	-21.57
Nha Trang, Vietnam	12.2	109.2	Taylor_Ranch_TWRS, ID, USA	45.01	-114.82
Lanzhou, China	36.0	103.0	NEON-Disney, CO, USA	28.01	-81.44
Pontianak, Indonesia	0.1	109.2	Monterey, Canada	36.59	-121.85
Pune, India	18.5	73.8	Tomsk, Russia	56.47	85.04
Sao Paulo, Brazil	-23.6	-46.6	Irkutsk, Russia	51.80	103.08
Omkoi, Thailand	17.8	98.4	Yekaterinburg, Russia	57.03	59.53
Cuiaba, Brazil	-15.6	-56.1	Ussuriysk, Russia	43.70	132.16
Cairo, Egypt	30.1	31.2	Amsterdam_Island	-37.80	77.58
Kaiping, China	22.4	112.7	ND_Marbel_Univ, Philippines	6.50	124.82
Penn State, PA, USA	40.8	-77.9	South_Pole, Antarctica	-89.99	77.30
Dhaka, Bangladesh	23.7	90.4	NASA/AFRC, CA, USA	34.58	-118.12
Mexico City, Mexico	19.0	-99.1	NASA/ARC, CA, USA	37.40	-122.07

Atmospheric
Measurement
Techniques
Open Access
Discussions

Table 3: For a network of 50 mini-LHR instruments, the knowledge of CO_2 fluxes improves significantly overland in all regions as well as globally, with the largest improvements in the Northern hemisphere. Numbers shown are the error reductions (γ) over integrated large-scale regions for winter and summer months respectively.

Overland regions	Seasonal range of γ	Median γ
Southern hemisphere	58%- 81%	65%
Tropics	47% - 76%	58%
Northern hemisphere	71% - 92%	81%
Global	64% - 91%	82%

5

Atmospheric
Measurement
Techniques
Discussions

Figure 1: The mini-LHR (right) is portable and can be deployed to remote locations where larger TCCON installations are not possible due to the fragile ground conditions. Here, the mini-LHR monitors XCO2 and XCH4 alongside an eddy covariance tower (left) in a collapse scar bog permafrost site in Alaska
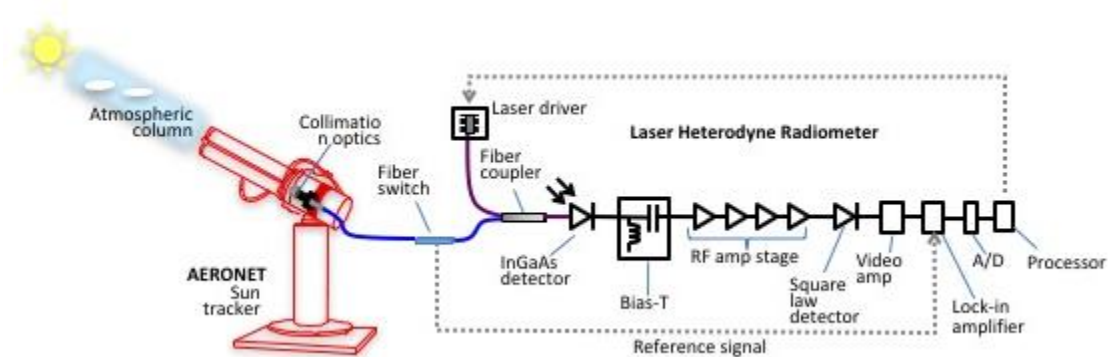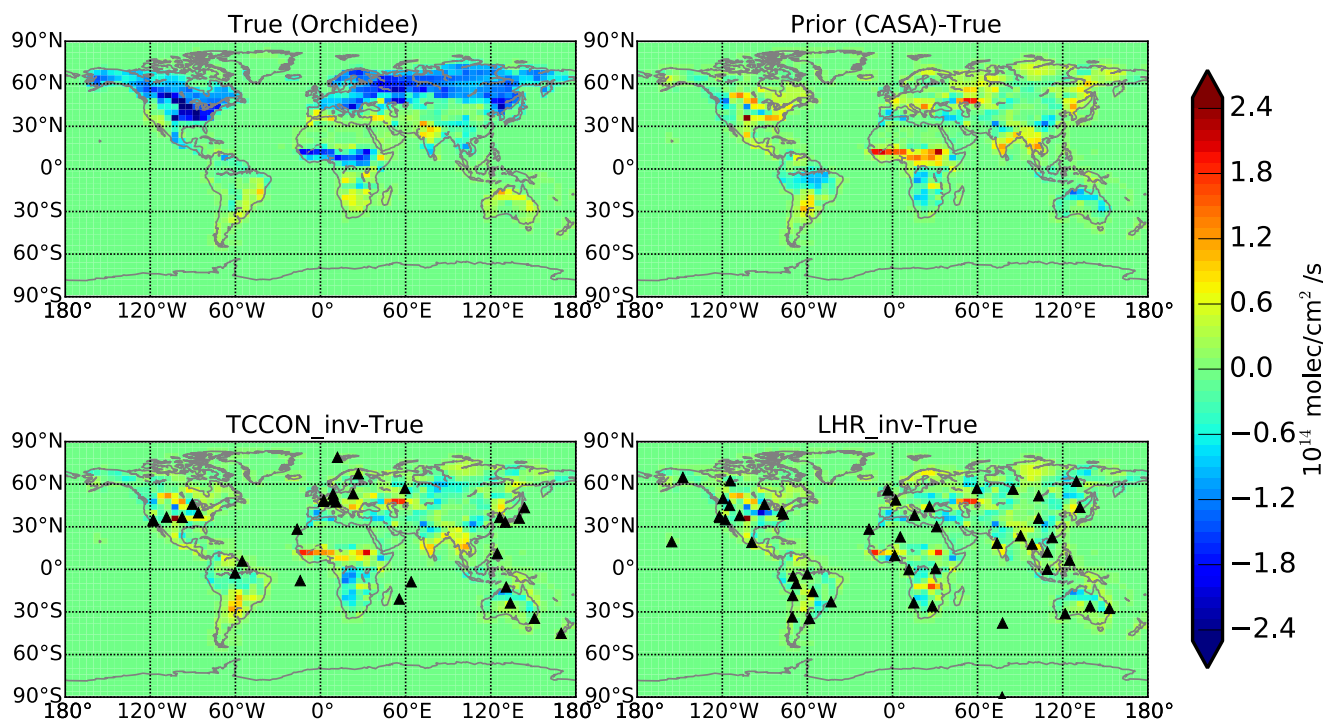

Figure 2: Schematic of a mini-LHR. Sunlight is collected with collection optics that are non-invasively connected to the AERONET sun tracker. Sunlight is then modulated with a fibre switch, superimposed with infrared laser light from a distributive feedback laser in a single mode fibre coupler, and mixed in a fast photoreceiver/InGaAs detector to produce a radio frequency (RF) beat signal. In the RF receiver (custom), a bias tee separates RF and DC outputs. The RF signal passes through a gain stage, and is then detected with a square-law detector. The signal is measured with a lock-in amplifier that is referenced to the modulation frequency as the laser scans across an absorption feature. A microprocessor controls the laser scanning and data collection.
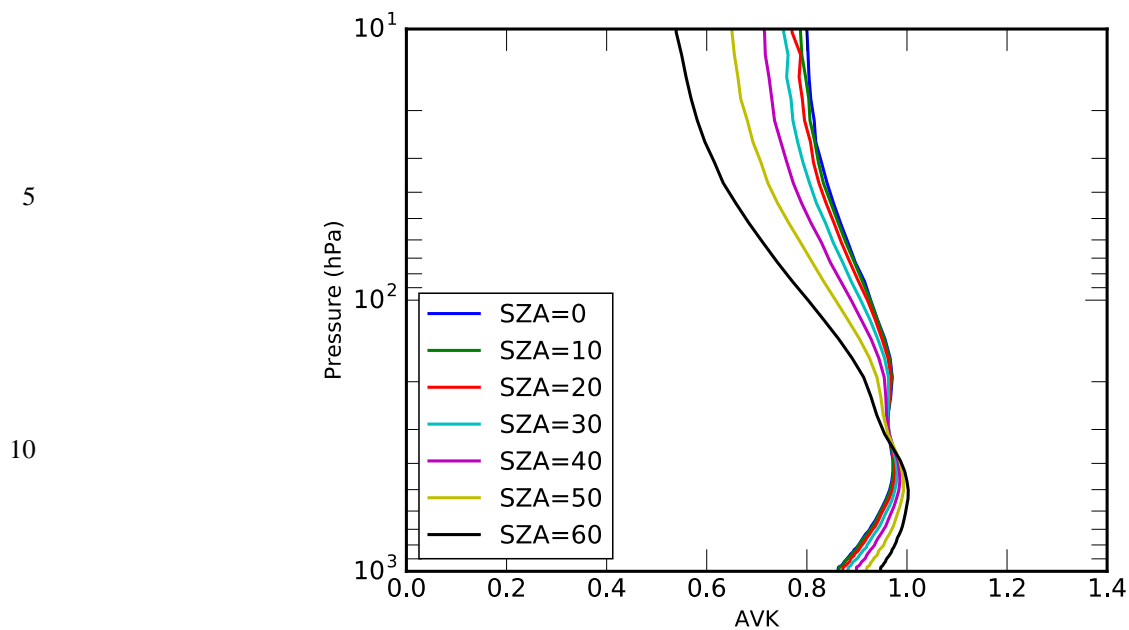
Figure 3: Averaging kernel ($\widehat{AK}$) values for CO_2 for different values of solar zenith angles. Calculations for CO_2 have been done assuming a mini-LHR SNR of 500 (although in reality SNR varies with SZA and is highest near a SZA of 0), and assuming a background variability of 5%.

Figure 4 Distribution of land biosphere CO_2 fluxes (10^{14} molec/cm^2/s) for July in our study year, described on the 4º latitude x 5 º longitude GEOS-Chem model grid. The top panels show (left) output from the ORCHIDEE land surface model that we use to define the true state, and (right) the difference between ORCHIDEE and the CASA model (used to define our *a priori* state). The bottom panels show the difference between the true state and a posteriori flux estimated inferred from CO_2 column measurements collected by (left) TCCON locations and (right) the enhanced mini-LHR network locations; the closed triangle symbols denote measurement locations for the (left) TCCON and (right) mini-LHR network.
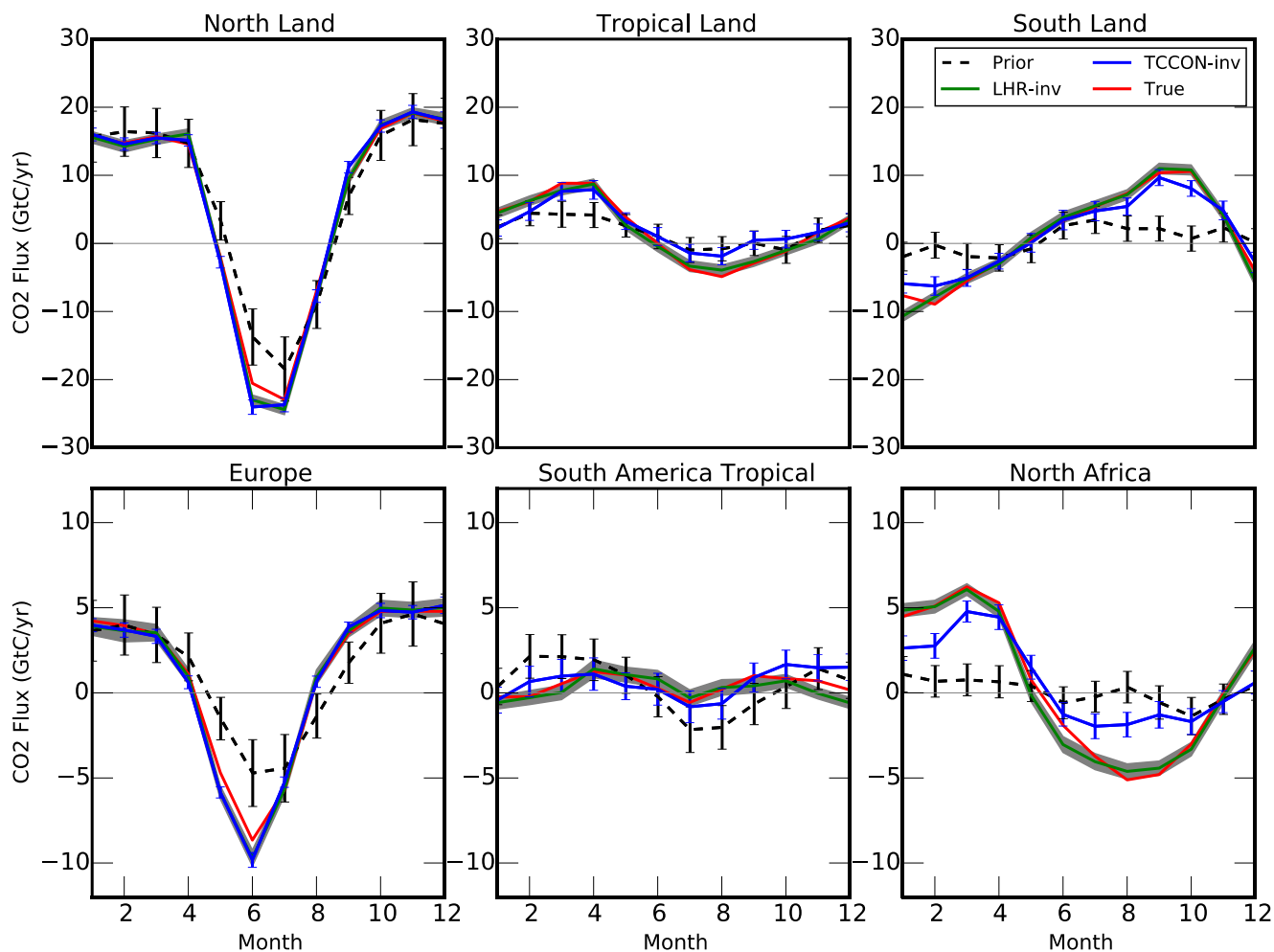
Figure 5 True, *a priori* **and** *a posteriori* **seasonal cycles of CO₂ fluxes (GtC/yr) over large-scale geographical regions, from our study year. Vertical lines superimposed on the (red)** *a priori* **fluxes and (blue)** *a posteriori* **fluxes inferred from TCCON data, and the shaded grey envelope on the (green)** *a posteriori* **fluxes from the mini-LHR data denote uncertainties associated with the values.**
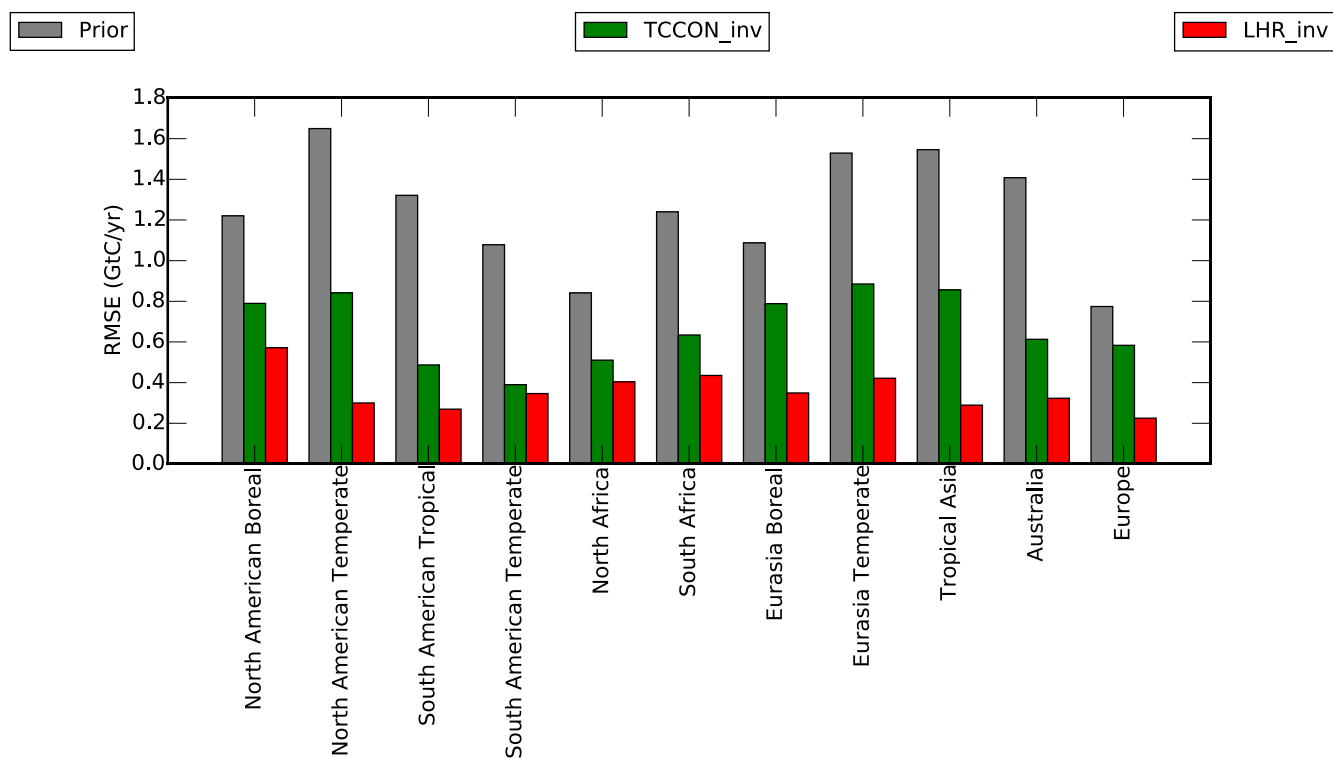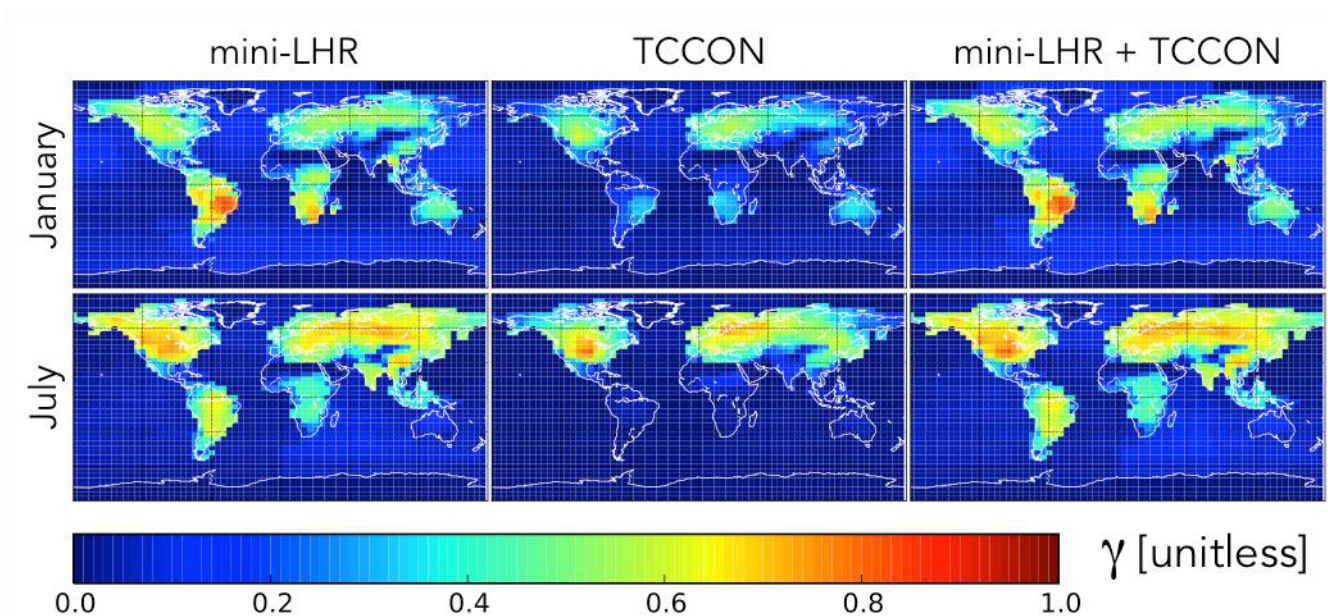
5

Figure 6 Annual mean root-mean-square errors (RMSE, GtC/a) of the *a priori* and the *a posteriori* flux estimates inferred for large-scale geographical regions from TCCON and mini-LHR CO₂ columns.

Figure 7: Theoretical improvement in the knowledge of CO_2 fluxes for a nominal (top) January and (bottom) July as determined by the γ factor, defined in the main text, for the (left) mini-LHR, (middle) TCCON, and (right) combined mini-LHR and TCCON measurement network.